A MULTI-RADAR JOINT BEAMFORMING METHOD

Oded Bialer [1] *and Sammy Kolpinizki* [1]

[1] General Motors - Advanced Technical Center Israel

ABSTRACT

In this paper a multi-radar beamforming algorithm is developed that attains higher angular resolution than the individual radars. The method is based on jointly processing the received signals from mutually non-coherent radars that are widely spaced on a vehicle. The proposed method can separate and discriminate between close targets, which are not separated by trilateration nor by filtering the multiple radars measurements.

1. INTRODUCTION

The automotive radar is a key sensor for enabling active safety and autonomous driving applications due to its relative large detection range, and robustness to adverse weather. These applications also require high spatial resolution so that close objects can be distinguished separately, and their position can be estimated accurately [1]-[2].

The azimuth angle resolution of an individual radar is limited by its aperture (diffraction limit). The radar angular resolution can be increased if multiple statistically independent realization are available by using super resolution sub-space methods such as Multiple Signal Classification (MUSIC) [3] or Minimum Variance Distortionless Response (MVDR) [4]. However, in many applications, such as the automotive radar case, there is only one observation vector per targets positions, and then sub-space methods cannot be applied unless spatial smoothing [5] is performed, which in turn reducing the radar aperture and its resolution.

Surround vehicle sensing requires to have multiple radars surrounding the vehicle. In this case there may be few widely spaced radars[1] sharing the same field-of-view (FOV), and thus jointly processing their information can improve the radars performance. Conventionally each radar performs independent targets detections and angles of arrival estimation based on independent beamforming, and then the estimations of all radars that share a common FOV are combined by Kalman filtering [6] or occupancy grid filtering [7]-[8]. This approach can improve the estimation accuracy when the targets are already separable by each individual radar, but cannot resolve false detections and bias in the estimations that occurs when the targets are closer than the spatial resolution of the individual radars.

At short target distances from the radars (short with respect to the radars spacing distance) the angles between the radars and each target differ significantly, and hence by trilateration of the radars measurements the spatial resolution can be improved compared to the angular resolution of each individual radar, and close targets can be separated. However, when the targets distance is larger than few tenths of meters (significantly larger than the radars spacing), and the radars range resolution is limited to tenths of centimeters (as if often the case in automotive radars) then the radars have similar observation angle to the target and hence trilateration results in insignificant resolution improvement.

The contribution of this paper is the development of a multi-radar beamforming method that attains higher angular resolution than the individual radars angular resolution by jointly processing the received signals from multiple radars, which are not mutually coherent. The proposed method can separate and discriminate between close targets at relatively large distance, which are not separated by conventional trilateration nor by filtering of the independent radar estimations.

2. SYSTEM MODEL

We consider a system of K radars, and M unknown close targets in the common field-of-view of the radars. The radars are widely spaced with respect to the wavelength, but not spaced apart enough with respect to the range resolution of the radars and therefore the targets cannot be separated by trilateration (i.e. by intersecting the range resolution cells of the radars). Each radar transmits and receives its own signal, and it is assumed that transmissions from different radars are separated by code, frequency, or time, such that they do not interfere. An illustrating of the system model for the case that $K = 2$, and $M = 3$ is depicted in Fig. 1.

The radars have the same antenna spacings, each has N receive antennas[2] horizontally linear spaced. The antenna elements of each radar are coherent among themselves, but are not coherent between radars. The radars perform standard range and Doppler filtering for each receive antenna [9]. As mentioned, it is assumed that the M targets are close and are

[1] Widely spaced with respect to the signal wavelength

[2] In MIMO N is the product of all transmit and receive antennas

not separated into different range and Doppler resolution cells of the radars (as shown in Fig. 1). The k-th radar received array response for the range and Doppler filter resolution cell of the targets can be expressed by

$$\boldsymbol{y}^k = \sum_{m=0}^{M-1} \boldsymbol{a}(\theta_m^k) s_m^k + \boldsymbol{v}^k, \tag{1}$$

where s_m^k and θ_m^k are the complex reflection coefficient and the angle of the m-th target, respectively, $\boldsymbol{v}^k$ is the noise vector, and

$$\boldsymbol{a}(\theta) = \begin{bmatrix} e^{\frac{j2\pi}{\lambda} x_1^k \sin(\theta)} \\ \vdots \\ e^{\frac{j2\pi}{\lambda} x_N^k \sin(\theta)} \end{bmatrix}, \tag{2}$$

is the array response (steering vector) for a target at angle θ, where λ is the wavelength, and x_i^k is linear spacing between the i-th array element and the k-th radar center position.

We consider the case where the angular difference between the targets is smaller than the angular resolution of each individual radar (smaller than the -3 dB angular width of the Bartlett beamformer main lobe). In this case, separating the targets is challenging since they are not separable by trilateration nor by Bartlett beamforming. In the next section, we derive a multi-radar beamforming algorithm that attains higher angular resolution than the individual radars Bartlett beamforming and hence can better separate close targets.

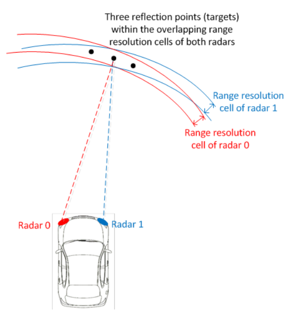

Fig. 1. Illustration of the system model with two radars and three reflection points that are within the intersection of the range resolution cells of the radars, and therefore are not separated by trilateration.

3. MULTI-RADAR JOINT BEAMFORMING

Next, we derive a multi-radar beamforming algorithm, based on the measurements, $\boldsymbol{y}^0, .., \boldsymbol{y}^{K-1}$. The multi-radar beamforming is calculated per a specific range and over a grid of azimuth angles, both are with respect to a fixed focal point position, which is chosen to be the center front point of the vehicle, as shown in Fig. 2. Denote by $\bar{\theta}$ the beamforming angle with respect to the focal point position, and by θ^k the corresponding angle from the k-th radar to that beamforming point, as shown in Fig. 2.

The proposed beamforming algorithm performs two stages per each angle. In the first stage a transformation is applied to the received signals $\boldsymbol{y}^0, .., \boldsymbol{y}^{K-1}$, which aligns their steering vectors angles of arrival. In the second stage the aligned vectors are further processed in order to focus their energy to the desired angle while minimizing the interferences from targets at other angles. Both stages will be further detailed next.

Referring to Fig. 2, let us consider a beamforming angle $\bar{\theta}$, and the corresponding angle θ^k being either θ^0 or θ^1. In the first stage of the algorithm for each received signal $\boldsymbol{y}^k$, a corresponding transformed vector, $\boldsymbol{z}_{\theta^k}$, is obtained by

$$\boldsymbol{z}_{\theta^k} = \boldsymbol{G}_{\theta^k} \boldsymbol{y}^k, \tag{3}$$

where

$$\boldsymbol{G}_{\theta^k} = \text{diag}\{\boldsymbol{a}(-\theta^k)\}, \tag{4}$$

and $\text{diag}\{\boldsymbol{x}\}$ is a diagonal matrix with the elements of the vector $\boldsymbol{x}$ along its diagonal. By substituting (1) and (4) into (3) we have that

$$\boldsymbol{z}_{\theta^k} = \sum_{m=0}^{M-1} \begin{bmatrix} e^{\frac{j2\pi}{\lambda} x_1^k (\sin(\theta_m^k) - \sin(\theta^k))} \\ \vdots \\ e^{\frac{j2\pi}{\lambda} x_N^k (\sin(\theta_m^k) - \sin(\theta^k))} \end{bmatrix} s_m^k + \boldsymbol{\eta}^k, \tag{5}$$

where $\boldsymbol{\eta}^k = \boldsymbol{G}_{\theta^k} \boldsymbol{v}^k$ is the noise vector.

We can further express the argument $\sin(\theta_m^k) - \sin(\theta^k)$ in (5) as

$$\begin{aligned} \sin(\theta_m^k) - \sin(\theta^k) &= \sin(\theta^k + \Delta_m) - \sin(\theta^k) = \\ &\sin(\theta^k)\cos(\Delta_m) + \cos(\theta^k)\sin(\Delta_m) - \sin(\theta^k), \end{aligned} \tag{6}$$

where $\Delta_m = \bar{\theta}_m - \bar{\theta}$ is the difference between the m-th target angle, $\bar{\theta}_m$, and the beamforming angle $\bar{\theta}$, both with respect to the focal point position. Assuming that the targets are close in angle and that the beamforming angle is focused close to the targets (i.e. focused to the area to interest) then $\cos(\Delta_m) \approx 1$. Assuming also that the targets angles are relatively small, i.e. $\theta^k \leq 45°$, then $\cos(\theta_m^k) \approx \cos(\bar{\theta}_m)$. From the latter two approximations we have that

$$\boldsymbol{z}_{\theta^k} \approx \sum_{m=0}^{M-1} \boldsymbol{b}(\Delta_m) s_m^k + \boldsymbol{\eta}^k, \tag{7}$$

where

$$\boldsymbol{b}(\Delta_m) = \begin{bmatrix} e^{\frac{j2\pi}{\lambda} x_1^k cos(\bar{\theta}_m) sin(\Delta_m)} \\ \vdots \\ e^{\frac{j2\pi}{\lambda} x_N^k cos(\bar{\theta}_m) sin(\Delta_m)} \end{bmatrix}. \tag{8}$$

From (7) it is realized that the transformed vectors $\boldsymbol{z}_{\theta^0}, \boldsymbol{z}_{\theta^1} .., \boldsymbol{z}_{\theta^{K-1}}$ are aligned in the sense that each is a different linear combination of approximately the same set of vectors $\boldsymbol{b}(\Delta_0), \boldsymbol{b}(\Delta_1), .., \boldsymbol{b}(\Delta_{M-}$

This important property does not exist in the original received signal $\boldsymbol{y}^0, \boldsymbol{y}^1.., \boldsymbol{y}^{K-1}$ (as realized from (1)), and will be used in the second stage of the beamformer, which will be detailed next.

The beamforming output for the angle $\bar{\theta}$ is given by

$$P_{\bar{\theta}} = min_{\boldsymbol{w}} \sum_{k=0}^{K-1} \left| \boldsymbol{w}^H \boldsymbol{z}_{\theta^k} \right|^2 \quad \text{subjected to } \boldsymbol{w}^H \mathbf{1} = 1, \tag{9}$$

where $\mathbf{1}$ is a N dimensional vector of ones. By substituting (7) into (9) we can express the beamforming output as

$$P_{\bar{\theta}} = min_{\boldsymbol{w}} \sum_{k=0}^{K-1} \left| \boldsymbol{w}^H \sum_{m=0}^{M-1} \boldsymbol{b}(\Delta_m) s_m^k + \boldsymbol{\eta}^k \right|^2 \quad \text{subjected to } \boldsymbol{w}^H \mathbf{1} = 1. \tag{10}$$

Next, we analyze the beamformer given in (10). Let us consider first the case that the beamforming angle is focused on a target angle, for example target angle index 0. Then $\Delta_0 = 0$, and $\boldsymbol{b}(\Delta_0) = \mathbf{1}$, hence from the constraint in (9) we have that $\boldsymbol{w}^H \boldsymbol{b}(\Delta_0) = 1$, and thus

$$\sum_{k=0}^{K-1} \left| \boldsymbol{w}^H \sum_{m=0}^{M-1} \boldsymbol{b}(\Delta_m) s_m^k + \boldsymbol{\eta}^k \right|^2 = \sum_{k=0}^{K-1} \left| s_0^k + \boldsymbol{w}^H \sum_{m=1}^{M-1} \boldsymbol{b}(\Delta_m) s_m^k + \boldsymbol{\eta}^k \right|^2. \tag{11}$$

In this case the desired signal is s_0^k, while the interference signal is $\sum_{m=1}^{M-1} \boldsymbol{b}(\Delta_m) s_m^k$, and the beamformer coefficients, $\boldsymbol{w}$, strive to minimize the interference energy. On the other hand, when the beamforming is not focused to a target angle then the beamforming output intensity will drop since there is only interference signal, which is minimized (nulled) by the beamformer.

The beamforming coefficients, $\boldsymbol{w}$, for angle $\bar{\theta}$ that solve (9) can be obtained using the Lagrange multiplier, which yields

$$\boldsymbol{w}_{\bar{\theta}} = \frac{\boldsymbol{R}_{\bar{\theta}}^{-1} \mathbf{1}}{\mathbf{1}^H \boldsymbol{R}_{\bar{\theta}}^{-1} \mathbf{1}}, \tag{12}$$

where

$$\boldsymbol{R}_{\bar{\theta}} = \sum_{k=0}^{K-1} \boldsymbol{z}_{\theta^k} \boldsymbol{z}_{\theta^k}^H. \tag{13}$$

By substituting (12) into (9) we obtain that the multi-radar beamforming output for angle $\bar{\theta}$ is given by

$$P_{\bar{\theta}} = \frac{1}{\mathbf{1}^H \boldsymbol{R}_{\bar{\theta}}^{-1} \mathbf{1}}. \tag{14}$$

The matrix $\boldsymbol{R}_{\bar{\theta}}$ has rank K, and hence is not invertible in the case that $K < N$. The rank of $\boldsymbol{R}_{\bar{\theta}}$ can be doubled when the array antenna elements are spaced symmetrically by applying forward-backward averaging [5] as follows

$$\boldsymbol{R}_{\bar{\theta}} = \sum_{k=0}^{K-1} \boldsymbol{z}_{\theta^k} \boldsymbol{z}_{\theta^k}^H + \hat{\boldsymbol{z}}_{\theta^k} \hat{\boldsymbol{z}}_{\theta^k}^H, \tag{15}$$

where $\hat{\boldsymbol{z}}_{\theta^k}$ is the vector $\boldsymbol{z}_{\theta^k}$ with reverse elements order. Furthermore, diagonal loading [12] can also be applied in order to insure solution stability when $\boldsymbol{R}_{\bar{\theta}}$ is ill-conditioned. In this case the beamforming output is given by

$$P_{\bar{\theta}} = \frac{1}{\mathbf{1}^H \left(\boldsymbol{R}_{\bar{\theta}} + \sigma^2 \boldsymbol{I} \right)^{-1} \mathbf{1}}, \tag{16}$$

where $\boldsymbol{I}$ is a diagonal matrix, and σ^2 is the diagonal loading parameter, which is chosen to be significantly lower than the maximal singular value of $\boldsymbol{R}_{\bar{\theta}}$.

We note that when the beamforming angle $\bar{\theta}$, is far from the targets, then the approximation in (7) does not hold. Meaning that each vector, $\boldsymbol{z}_{\theta^k}$ will be composed from a different set of vectors. However, in this case the beamforming output energy will anyhow be low since there will be low correlation between $\boldsymbol{z}_{\theta^k}$ and the vector of all ones $\mathbf{1}$, and hence due to the constraint that $\boldsymbol{w}^H \mathbf{1} = 1$ there will also be low correlation between $\boldsymbol{z}_{\theta^k}$ and $\boldsymbol{w}$, resulting in small $P_{\bar{\theta}}$ (as realized from (9)).

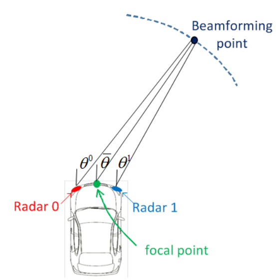

Fig. 2. Illustration of focal point position, radars positions and the angles $\bar{\theta}, \theta^k$

4. RESULTS AND DISCUSSION

We first demonstrate the developed multi-radar beamformer performance with simulation. The simulation included two radars spaced by 1m, each radar had 1 transmit and 8 receive antennas that where uniformly linearly spaced by half a wavelength. Two close targets at 50m distance were simulated, and the targets angles were 5 and 10 degrees with respect to the center point between the two radars. Each radar had a single observation vector with SNR per element of 30 dB. Fig. 3 shows the results of the multi-radar beamformer given in (16) compared to the Bartlett beamforming [5] of each one of the individual radar. The beamwidth of each independent radar[3]

[3]where beamwidth is considered here as the width between the -3dB points from the peak

is only 16 degrees, and hence it cannot separate the two targets, which are spaced by 5 degrees. On the other hand the multi-radar beamforming does manage to separate the two targets and estimate their angles accurately.

We have also tested the multi-radar beamformer with real-life measurements from two 77 GHz LFM radars. Each had a bandwidth of 750 MHz, 1 transmit and 8 receive antennas uniformly linearly spaced by half a wavelength. The tested scenario is illustrated in Fig. 4. The two radars were static and spaced by 1m and there were two static pedestrians spaced by 2m facing the radars. The range resolution cells of both radars are overlapping at the distance of the pedestrians as shown in Fig. 4, hence the pedestrians cannot be separated by trilateration. Furthermore, the angular separation of the pedestrians is 14 degree[4], and the 3 dB beam width resolution of each radar is only 16 degrees. At the receiver of each radar we have applied standard LFM range filtering by Fast Fourier Transform [9]-[10] and then the multi-radar beamformer was applied to each range bin of 10 cm separately.

In Fig. 5, we present in cartesian coordinates the multi-radar beamforming intensity over a span of range bins, where per each range bin only the intensity (in dB scale) of the beamforming peaks that were detected above the noise level are plotted. The true pedestrians positions are marked with a white x symbol. For a comparison we show in Fig. 6 the detected peaks of the independent Bartlett beamforming of both radars. It is observed that the Bartlett beamformers do not manage to separate the two close pedestrians, and as a result have false detections in between the pedestrians. On the other hand, the multi-radar beamformer obtains higher angular resolution and does manage to sperate the two targets with relatively accurate detections.

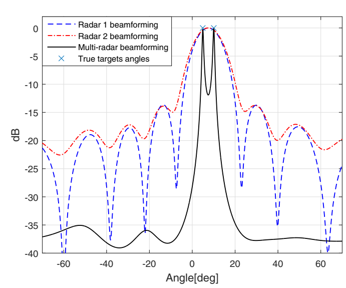

Fig. 3. Simulation Beamforming results for 2 radars spaced by 1m and two targets at 50m and angles of 5 and 10 degrees w.r.t center point between radars.

5. CONCLUSIONS

In this paper we developed a beamforming method that jointly processes the received array responses of multiple radars, which are not mutually coherent. The beamformer attained a significantly better angular resolution than the angular resolution of each individual radar. It manages to separating close targets even when the radars range resolution cells overlap and the targets cannot be separated by trilateration. The improved ability to separate close targets provides more accurate estimation of the true targets and eliminates false detections between close targets.

[4] with respect to the center point between the radars

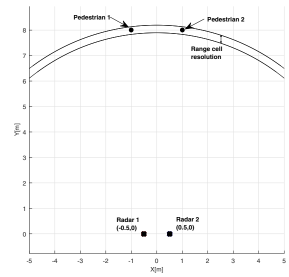

Fig. 4. Test scenario bird's-eye view

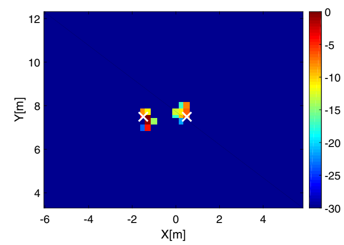

Fig. 5. Intensity of detected peaks in the Multi-radar beamforming output per each range bin of 10 cm and over a span of ranges, plotted in cartesian coordinates. Intensity color scale is in dB. The true pedestrians positions are marked with the white x symbol.

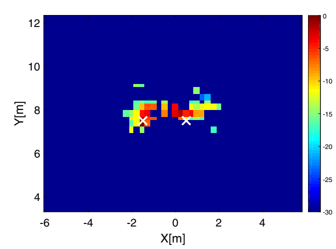

Fig. 6. Combined intensity of detected peaks in the Bartlett beamforming of the individual radars per each range bin of 10 cm and over a span of ranges, plotted in cartesian coordinates. Intensity color scale is in dB. The true pedestrians positions are marked with the white x symbol.

6. REFERENCES

[1] M. Heuer, A. Al-Hamadi, M.M. Meinecke, R. Mende, "Requirements on Automotive Radar Systems for Enhanced Pedestrian Protection," *19th International Radar Symposium*, May. 2012.

[2] R. H. Rasshofer and K. Naab, "77 GHz Long Range Radar Systems Status, Ongoing Developments and Future Challenges", *European Radar Conference*, EURAD 2005.

[3] P. Stoica and A. Nehorai, "MUSIC, Maximum Likelihood, and Cramer Rao Bound, *IEEE Trans. On Acoustics, Speech and Signal Processing*, May 1989, Dec. 1990.

[4] J. Capon, High Resolution Frequency-Wavenumber Spectrum Analysis, Proc. IEEE, Aug. 1969

[5] H.L. Van Trees, Optimum Array Processing, Wiley and Sons, 2002

[6] D. Lerro, Y. Bar-Shalom, "Tracking With Debiased Consistent Converted Measurements Versus EKF," *IEEE Trans. On Aerospace and Electronic Systems*, Vol. 29, No. 3, July 1993

[7] M. E. Bouzouraa, and U. Hofman, "Fusion of Occupancy Grid Mapping and Model Based Object Tracking for Driver Assistance Systems using Laser and Radar Sensors," *IEEE Intelligent Vehicles Symposium*, June 2010.

[8] R. G. Danescu, "Obstacle Detection Using Dynamic Particle-Based Occupancy Grids," *International Conference On Digital Image Computing Techniques and Applications (DICTA)*, 2011.

[9] W. L. Melvin, J. A. Scheer, Principles Of Modern Radar, Scitech Publishing 2013.

[10] V. Winkler, "Range Doppler detection for automotive FMCW radars," *The 4th European Radar Conference*, Oct. 2007

[11] A. B. Gershman and V. T. Ermolaev "Optimal Subarray Size for Spatial Smoothing," *IEEE Signal Processing Letters*, Vol. 2. No. 2, Feb. 1995

[12] J. Li, P. Stoica, Z. Wang "On Robust Capon Beamforming and Diagonal Loading," *IEEE Trans. On Signal Processing*, Vol. 51. No. 7, July 2003